Rev.Adv.Mater.Sci. 7 (2004) 108-125

OPTICS OF METAL NANOPARTICLES FABRICATED IN ORGANIC MATRIX BY ION IMPLANTATION

A.L. Stepanov[1] and R.I. Khaibullin[2,3]

[1]Institute for Experimental Physics and Erwin Schrödinger Institute for Nanoscale Research, Karl-Franzens-University Graz, A-8010 Graz, Austria
[2]Kazan Physical-Technical Institute, Russian Academy of Sciences, Sibirsky Trakt 10/7, 420029 Kazan, Russian Federation
[3]Gebze Institute of Technology, 41400 Gebze, Turkey

Received: June 21, 2004

Abstract. The present review concentrates on the fabrication of metal nanoparticles in polymer matrix by ion implantation. This approach is particularly promising for the development of optical composite materials in the production technology. Some examples on ion implantation into different polymer matrix are presented. Solid state and viscous polymer layers were irradiated by Ag^+ ions with doses up to $1.0 \cdot 10^{17}$ ion/cm^2. The composites were examined by various methods: Rutherford backscattering (RBS), transmission electron microscopy (TEM) and optical spectroscopy. As follows from electron microscopy and electron microdiffraction data, ion implantation is suited for creation of silver nanoparticles in the near-surface polymer layer. The optical density spectra taken for some of these composites demonstrate that the silver nanoparticles exhibit unusually weak and wide plasmon resonance spectra. The formation of silver nanoparticles in solid polymer layers carbonized by ion irradiation is considered. Based on the Mie theory, optical extinction spectra for metal particles in the polymer and carbon matrices are simulated and compared with optical spectra for complex silver core–carbon sheath nanoparticles. It was shown that the implantation into viscous polymer leads to less carbonization of matrix than in the case of solid substrate. The physics behind experimental optical spectra of the composite is discussed.

1. INTRODUCTION

At modern time, material engineering press towards providing smaller technological devices at the nanometer scale than are currently available in microelectronics. Therefore, there is a practical interest in the composites consisting of dielectrics (glasses, ion crystals, minerals, polymers etc.) with metal nanoparticles (MN), which is motivated by potential optical applications such as magnetooptic data storages, nonlinear optical switches, directional connectors, and so on. For example, the nonlinear optical properties of these composites stem from the dependence of their refractive index on incident light intensity. This effect is associated with MN, which exhibit an enhancement of local electromagnetic field in a composite and, as consequence, a high nonlinear susceptibility of the third order when exposed to ultrashort (picosecond or femtosecond) laser pulses [1]. It is well known [2] that such a local field enhancement stimulates a linear optical absorption of NM called as surface plasmon resonance (SPR). The electron transitions responsible for plasmon absorption in MN cause also a generation of an optical nonlinearity of a composite in the same spectral range. As a result, the manifestation of nonlinear optical properties is most efficient for wavelengths near the position of a SPR maximum. In practice, to reach the strong linear absorption of a composite in the SPR spectral region, attempts are made to increase the concentration (filling fac-

Corresponding author: A.L. Stepanov, e-mail: andrey.stepanov@uni-graz.at ; anstep@kfti.knc.ru

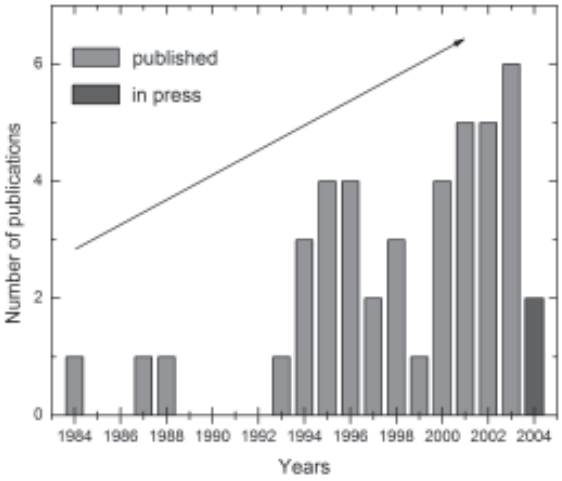

Fig. 1. Attendance of papers in the literature on synthesis of metal nanoparticles in polymer matrix by ion implantation until 2004 year.

tor) of MN. Systems with a higher filling factor offer a higher nonlinear susceptibility, when all other parameters of composites being the same [1].

Between suitable dielectrics as a container for MN, the organic matrix or polymer is of current interest. Nanoparticles may be embedded in a polymer in a variety of ways. These are chemical synthesis in an organic solvent [2], vacuum deposition on viscous-flow polymers [3], plasma polymerization combined with metal evaporation [4], *etc*. However, they all suffer from disadvantages, such as a low filling factor of metal or a wide distribution in size and shape of synthesized MN, which offsets the prospective optical properties of composites.

One of the most promising enhanced fabrication methods is ion implantation [5] because it allows reaching a high metal filling factor in an irradiated matrix beyond the equilibrium limit of metal solubility and provides controllable synthesis of MN at various depths under the surface. Despite the intensive study of MN synthesis by ion implantation in dielectrics, such as crystals and non-organic glasses which was started in 1973 by J. Davenas *et al.* with Na and K ions [6] and in 1975 by G.W. Arnold with Au ions [7], the formation of nanoparticles in organic matrices was realized only at the beginning of the eighties by N.C. Koon *et al*. in their experiments on irradiation of polymers by Fe ions [8] (1984). By implantation, it is possible to produce almost any metal–insulator (specifically, metal–polymer) composites, the support for this statement can be seen in Table 1, which gives a comprehensive list of references by 2004 year [9–48] and the information about type of MN, their shapes, and implantation conditions for various organic matrices.

As seen in a diagram (Fig. 1), a number of publications on MN fabrication in polymer by ion implantation increases during last years continuously. Falsely, in some publications, for examples [37,47], authors believed that there are only a few papers about metal ion implantation into polymer and gave references to almost themselves only. Table 1 and Fig. 1 demonstrate clearly the wide interest in the study of this topic by a number of scientific groups in the world where, at present time, the most active ones are in Kazan Physical-Technical Institute of the Russian Academy of Sciences, Göteborg University and Chalmers University of Technology (Sweden), Institute of Physical and Chemical Research (Japan), Beijing Normal University, and Beijing Radiation Center (China) and National Institute for Materials Science (Japan).

Present work focuses on polymer-based optical materials containing MN characterized by SPR. Note that noble metals exhibit the most pronounced SPR effect and, hence, the highest nonlinearity of the MN optical properties in insulators [2]. Only recently similar composite materials were fabricated by Ag^+ implantation into polymethylmethacrylate (PMMA) in 1994 [21,43-45] and epoxy resins in 1995 [40]. Therefore, the aim of this work is to study the SPR-related linear optical properties of MN introduced into a polymer matrix by implantation. For comparison of experimental optical spectra of silver nanoparticles synthesized by implantation in PMMA, calculated spectra based on the Mie classical electrodynamic theory were developed [2, 49]. Additional experimental data are presented to discuss the optical features of MN in irradiated polymer.

2. EXPERIMENTAL PROCEDURE

Thin PMMA and silicone polymer resin layers, which are optically transparent in a wide spectral range of 400–1000 nm [22,50] were used as substrates. Polymers were implanted by 30 keV Ag^+ ions with doses in the range from $3.1 \cdot 10^{15}$ to $10 \cdot 10^{17}$ ion/cm^2 at ion current density of 4 μA/cm^2 in a vacuum of 10^{-6} Torr using an ILU-3 ion implanter. In a control experiment, Xe- and Ar-ion implantation into polymers at the same conditions was performed. Various conditions of silicone polymer such as solid state and viscous state with the dynamic viscosity value of 20 Pa s were used.

Spectra of optical density were measured from 300 to 900 nm at room temperature in air using a dual beam spectrophotometer Hitachi 330. All spec-

Table 1. Conditions for MN synthesis by ion implantation into poly (ethyleneterephthalate) (PET), polyvinylidene fluoride (PVF_2), polyimide (PI), polymethylmethacrylate (PMMA), polymethylmethacrylate with phosphorus-containing fragments (PMMA + PF), polyethylene (PE), silicone polymer (phenylmethyl-silane resin with tin diethyldicaprilate) (SP), epoxy resin (ER), polyethylene high-density (PE-HD), polycarbonate (PC), polystyrene (PS) and polyetherimide (PEI). (Abbreviations – FMR, ferromagnetic resonance; TEM, transmission electron microscopy; AFM, atomic-force microscopy; OS, optical spectroscopy; and XRD, X-ray diffraction).

Metal of particles	*Matrix*	*Ion beam energy*, keV	*Ion dose,* ion/cm^2	*Ion current density*, μA/cm^2	*Substrate temperature*, K	*Shape of particles*	*Methods of particle determination*	*Authors*
Ti	PET	40 65	$2.0 \cdot 10^{17}$ $5.0 \cdot 10^{16}$	4.5		Spherical	TEM XRD	Wu *et al.* 2001 [9] Zhang *et al.* 2001 [10]
Cr	PET	40	$1.0 \cdot 10^{17}$	4.5			TEM XRD	Wu *et al.* 2000 [11]
Fe	PE	25	$(0.1\text{-}1.0) \cdot 10^{17}$	–	300		FMR	Koon *et al.*1984 [8]
Fe	PET	100-150	$(0.1\text{-}1.0) \cdot 10^{17}$	0.1-5	300	Spherical	TEM	Ogawa 1988 [12]
Fe	PET	40	$(1.0\text{-}3.0) \cdot 10^{16}$	1 – 6	300	needle-like	FMR FMR	Petukhov *et al.* 2001 [13]
Fe	PI	100-150	$(0.1\text{-}1.0) \cdot 10^{17}$	0.1-5	300	Spherical	TEM	Ogawa 1988 [12]
Fe	PI	40	$(0.3\text{-}1.2) \cdot 10^{17}$	4, 8, 12	300	Spherical and their aggregates	TEM FMR	Khaibullin R.I. *et al.* 2002 [14] Popok *et al.* 2002 [15] 2003 [16] Rameev *et al.* 2003 [17]
Fe	PMMA	100-150	$(0.1\text{-}1.0) \cdot 10^{17}$	0.1-5	300	Spherical	TEM	Ogawa 1988 [12]
Fe	PMMA	40	$(0.1\text{-}6.0) \cdot 10^{17}$	1 – 10	300	Spherical and their aggregates	TEM FMR	Petukhov *et al.* 1993 [18] 1995 [19] 1996 [20] 2001 [13] Bazarov *et al.* 1995 [21]
Fe	PMMA-PF	40	$(1.0\text{-}3.0) \cdot 10^{16}$	1 – 6	300	Spherical and their aggregates	TEM FMR	Petukhov *et al.* 2001 [13]
Fe	PVF_2	25	$(0.1\text{-}1.0) \cdot 10^{17}$	–	300		FMR	Koon *et al.* 1984 [8]
Fe	Silicone polymer	40	$(0.3\text{-}1.8) \cdot 10^{17}$	4	300	Spherical and their aggregates	TEM	Khaibullin R.I. *et al.* 1998 [22] 1999 [23] 2000 [24] 2003 [25] Rameev *et al.* 2000 [26]

Co	ER	40	$(0.3\text{-}2.5)\cdot10^{17}$	2-8	300	Spherical, needle-like, drop-like,cubic-faced and so on.	TEM	Stepanov *et al.* 1994 [27] 1995 [28] Abdulin *at el.* 1996 [29] 1996 [30] 1998 [31] Khaibullin R.I. *et al.* 1996 [32] Khaibullin I.B. *et al.* 1997 [33]
Co	PI	100-150	$(0.1\text{-}1.0)\cdot10^{17}$	0.1-5	300	Spherical	TEM	Ogawa 1988 [12]
Co	PI	40	$(0.3\text{-}1.5)\cdot10^{17}$	4, 8, 12	300	Spherical and their aggregates	TEM	Popok *et al.* 2002 [15] 2003 [16] Rameev *et al.* 2003 [17] 2004 [34]
Co	Silicone polymer	40	$(0.3\text{-}1.8)\cdot10^{17}$	4	300	Spherical and their aggregates	TEM FMR	Khaibullin R.I. *et al.* 2000 [24] Rameev *et al.* 2000 [26]
Ni	Nylon	69	$2.0\cdot10^{17}$	4.5	–	Spherical	TEM	Zhang *et al.* 2001 [10]
Ni	PET	69	$(1.0\text{-}2.0)\cdot10^{17}$	4.5	–	Spherical	TEM X-ray	Zhang *et al.* 2001 [10]
Cu	PC	60	$(1.0\text{-}3.0)\cdot10^{17}$	1-3	–	Spherical	TEM AFM, OS	Umeda *et al.* 2003 [35] Boldyryeva *et al.* 2004 [36]
Cu	PE-HD	60	$(1.0\text{-}1.5)\cdot10^{17}$	1	–	Spherical	TEM OS	Umeda *et al.* 2003 [35]
Cu	PET	40	$(0.5\text{-}2.0)\cdot10^{17}$	4-5	360	Spherical	TEM AFM XRD	Wu *et al.* 2000 [11] 2001 [38] Zhang *et al.* 2001 [10]
Cu	PET	40	$(1.0\text{-}3.0)\cdot10^{16}$	1–6	360	Spherical	TEM	Petukhov *et al.* 2001 [13]
Cu	PI	150	$(0.5\text{-}1.0)\cdot10^{17}$	1-5	< 360	Spherical	TEM	Yushida and Iwaki 1987 [39]
Cu	PI	80 100	$5.0\cdot10^{16}$	0.1	< 630	Spherical	TEM	Kobayashi *et al.* 2001 [40]
Cu	PMMA	40	$(0.1\text{-}6.0)\cdot10^{17}$	1– 6	360	Spherical	TEM	Petukhov *et al.* 2001 [13]
Cu	PMMA-PF	40	$(1.0\text{-}3.0)\cdot10^{16}$	1–6	360	Spherical	TEM	Petukhov *et al.* 2001 [13]
Zn	PI	150	$5.0\cdot10^{17}$	1-5	< 360	Spherical	TEM	Yushida and Iwaki 1987 [39]

Pd	PI	100	$(0.1\text{-}1.0)\cdot10^{17}$	0.1	< 630	Spherical	TEM	Kobayashi *et al.* 2001 [40]
Ag	ER	30	$(0.2\text{-}7.5)\cdot10^{17}$	4	300	Spherical	TEM OS	Stepanov *et al.* 1995 [41] 1997 [42] Khaibullin I.B. *et al.* 1997 [33]
Ag	PC	60	$(0.6\text{-}3.0)\cdot10^{17}$	3	–	Spherical	TEM AFM, OS	Boldyryeva *et al.* 2004 [36]
Ag	PET	79	$(0.5\text{-}2.0)\cdot10^{17}$	4.5	–	Spherical	TEM	Wu *et al.* 2000 [11] 2001 [9] 2002 [43] Zhang *et al.* 2001 [10]
Ag	PM	130	$(0.1\text{-}5.0)\cdot10^{17}$	1–3	< 630	Spherical	TEM	Kobayashi *et al.* 2001 [40]
Ag	PMMA	30	$(1.0\text{-}7.5)\cdot10^{16}$	4	300	Spherical	TEM OS	Stepanov *et al.* 1994 [44] 2000 [45] 2002 [46] Bazarov *et al.* 1995 [21]
Ag	Silicone polymer	30	$(0.6\text{-}1.8)\cdot10^{17}$	4	300	Spherical and their aggregates	TEM OS	Khaibullin R.I. *et al.* 1998 [22] 1999 [23] Stepanov *et al.* 1998 [47]
W	PET	136	$1.0\cdot10^{17}$	–	–	Spherical	TEM	Wu *et al.* 2003 [48]
Pt	PC	106	$1.0\cdot10^{17}$	–	–	Spherical	TEM	Rao *et al.* 1994 [49]
Pt	PEI	106	$1.0\cdot10^{17}$	–	–	Spherical	TEM	Rao *et al.* 1994 [49]

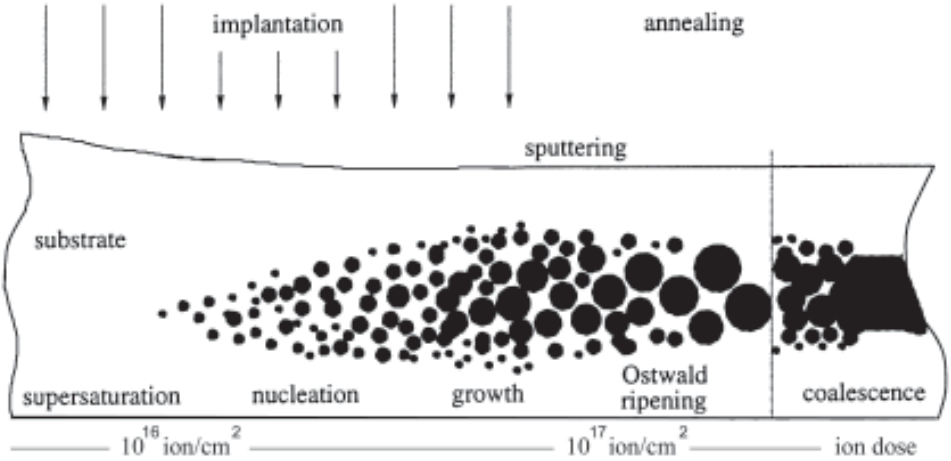

Fig. 2. Basic physical stages of nanoparticle synthesis by ion implantation in dependence on ion dose.

tra were recorded in a standard differential mode in order to normalize substrate effects. The samples obtained were examined with transmittance electron microscopy (TEM) by Tesla BM-500 microscope and with Rutherford backscattering (RBS) using a beam of 2 MeV $^4He^+$ ions with van de Graff accelerator.

Optical spectra of spherical MN embedded in various dielectric media were simulated in terms of the Mie electromagnetic theory [49], which allows one to estimate the extinction cross section σ_{ext} for a wave incident on a particle. This value is related to the light intensity loss ΔI_{ext} of an incident light beam I_0 passing through a transparent particle-containing dielectric medium due to absorption σ_{abs} and elastic scattering σ_{sca}, where $\sigma_{ext} = \sigma_{abs} + \sigma_{sca}$. Following the Lambert-Beer law

$$\Delta I_{ext} = I_0\left(1 - e^{-C\sigma_{ext}h}\right), \quad (1)$$

where h is the thickness of the optical layer and C the density of nanoparticles in a sample. The extinction cross section is connected to the extinction constant γ as $\gamma = C\sigma_{ext}$.

Experimental spectral dependencies of optical density (*OD*) are given by

$$OD = -\lg\left(\frac{I}{I_0}\right) = \gamma h \lg(e), \quad (2)$$

hence, for samples with electromagnetically non-interacting nanoparticles, it is possible to put $OD \sim \sigma_{ext}$. Therefore, experimental *OD* spectra can be compared with model spectral dependences that are expressed through σ_{ext} found from the Mie theory.

3. ION SYNTHESIS OF METAL NANOPARTICLES IN DIELECTRIC MATRIX

Ion implantation is an effective tool for introducing single impurities into the surface layer to a depth of several micrometers [5]. The surface modification of the material depends on its properties, as well as on ion implantation parameters (ion type and energy, ion current density, target temperature, *etc.*). A critical implantation parameter is ion dose F_0, which determines the implant amount. Depending on the modification of an insulating target (polymers, inorganic materials, ionic crystals, minerals, *etc.*), ion implantation may be conventionally divided into low-dose and high-dose implantation (Fig. 2). In the former case ($F_0 \leq 5.0 \cdot 10^{14}$ ion/cm^2), the stopped ions are disperse (isolated from one another) in the insulating matrix. The energy of ions implanted is transferred to the matrix through the excitation of electronic shells (ionization) and nuclear collisions. This causes radiation-induced defects, which, in turn, may reversibly or irreversibly modify the material structure [5]. Various types of polymer structure damage have been observed [51]: breaking of covalent bonds in macromolecules, generation of free radicals, cross linkage, oxidation and carbonization of irradiated layers, formation of new chemical bonds between atoms of the insulator or between ions implanted, *etc*. In addition, ion implantation may be accompanied by the intense sputtering of the surface exposed [42, 52] or, sometimes, by the swelling of the polymer [16,53].

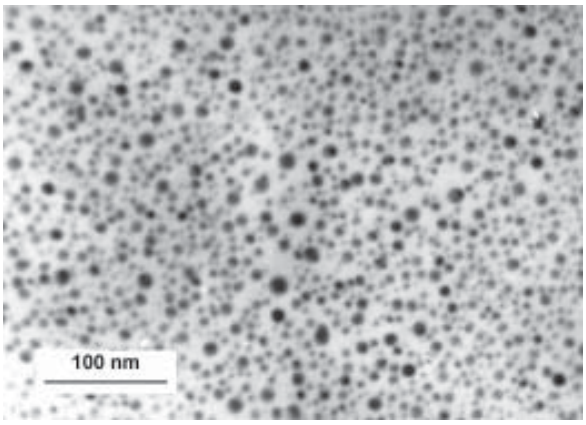

Fig. 3. Micrograph of silver nanoparticles produced by Ag^+ implantation into PMMA at a dose of $5.0 \cdot 10^{16}$ ion/cm^2 [44].

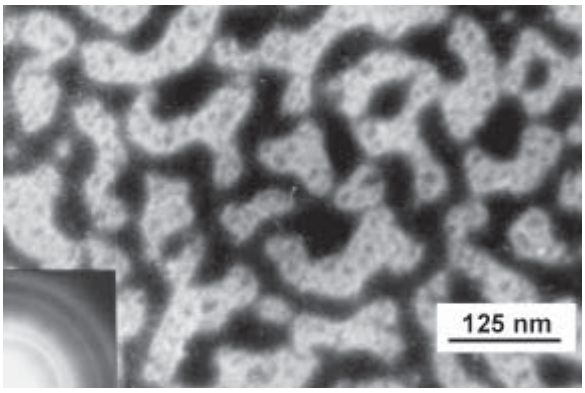

Fig. 4. Micrograph of cobalt labyrinth structures produced by Co^+ implantation into viscous epoxy resins at a dose of $2.5 \cdot 10^{17}$ ion/cm^2 [28].

High-dose implantation may also be divided into dose (or time) stages (Fig. 2). At F_0 between 10^{15} and 10^{17} ion/cm^2, the equilibrium solubility of metallic implants in insulators (in particular, polymers) is usually exceeded, causing the nucleation and growth of MN (Fig. 3). The dose threshold value depends on the type of the insulator and implant. For 25-keV silver ions implanted into $LiNbO_3$, the threshold dose was found to be $F_0 \approx 5.0 \cdot 10^{15}$ ion/cm^2 [54], but for 30-keV silver ions implanted into epoxy resin, $F_0 \approx 10^{16}$ ion/cm^2 [40]. As mentioned in [16], a ultra-dispersed magnetic phase in polyimide was shown to form under doses as high as $\approx 10^{17}$ ion/cm^2 at 40 keV Fe-irradiation.

At the next stage of high-dose implantation, starting from $F_0 \geq 10^{17}$ ion/cm^2, the existing MN coalesce to form MN aggregates or quasi-continuous films in the surface layer (Fig. 2). For example, the irradiation of epoxy resin by 40-keV cobalt ions at higher-than threshold doses favors the formation of thin labyrinth structures (Fig. 4) [28, 29,31,32]. The MN distribution established in the insulator after coalescence or Ostwald ripening may be disturbed by postimplantation thermal or laser annealing.

In this work, composites where MN are disperse and isolated from each other, i.e., synthesized at ion doses of 10^{15}–10^{17} ion/cm^2 in PMMA, were studied. In present case of implantation by heavy Ag^+ ions at relatively low energy of 30 keV, nuclear collisions prevail during interaction of accelerated ions with atoms of insulator. They displace atoms in the polymer matrix and break some chemical bonds of substrate. Along with this, target atoms effectively lose electrons and the implanted Ag^+ ions deionize with the formation of neutral silver atoms (Ag^0). In principle, Ag atoms may combine with arising organic radicals and polymer ions or take part in the oxidation reaction. However, because of a great difference in Gibbs free energy between Ag atoms and atoms of PMMA elements, Ag–Ag bonding is energetically more favorable.

The formation of MN proceeds in several stages: the accumulation of and subsequent supersaturation by Ag^0 atoms in a local surface region of the polymer, the formation of nuclei consisting of several atoms, and the growth of silver particles from the nuclei. Assuming that the nanoparticles nucleate and grow via the successive attachment of silver atoms (which are neutralized by embedded Ag^+ ions), one may conclude that this process is governed simultaneously by the diffusion coefficient and local concentration of silver atoms, i.e., depends on the matrix temperature. In this work, ion implantation was performed under identical conditions; specifically, the polymer during irradiation was kept at room temperature.

As follows from electron microscopy data, silver ion implantation under the experimental conditions considered results in the formation of silver nanoparticles in PMMA. For example, the cross-sectional micrograph in Fig. 2 and plane view in Fig. 3 (a dose of $5.0 \cdot 10^{16}$ ion/cm^2) shows dark spherical nanoparticles against the bright field (polymer). The irradiation of PMMA by xenon ions did not result in such patterns. Microdiffraction patterns demonstrate that the nanoparticles have the fcc structure of metallic silver. The patterns consist of thin rings (corresponding to polycrystalline nanoparticles) imposed

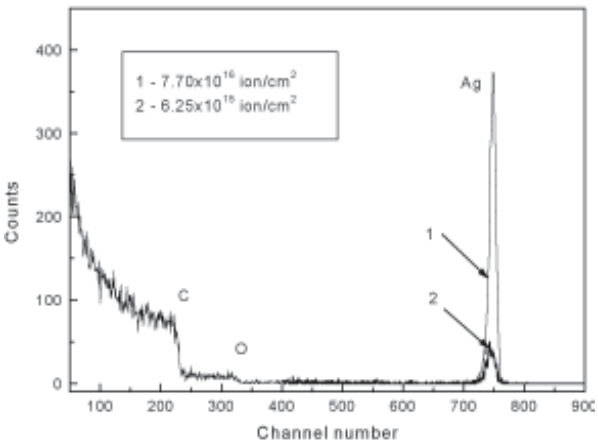

Fig. 5. RBS spectra from PMMA irradiated by silver ions for doses of (1) $7.7 \cdot 10^{16}$ and (2) $6.25 \cdot 10^{15}$ ion/cm^2 [44].

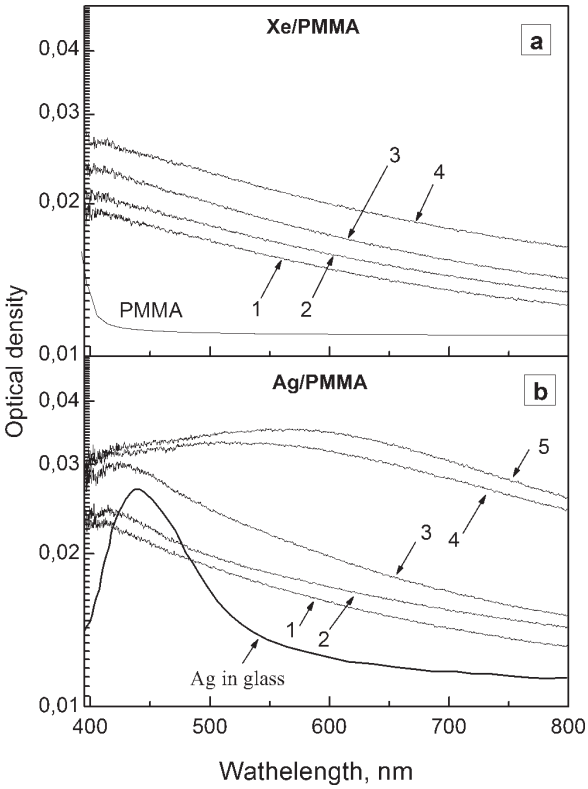

Fig. 6. Experimental optical density spectra from PMMA irradiated by(a) xenon and (b) silver ions for doses of (1) $0.3 \cdot 10^{16}$, (2) $0.6 \cdot 10^{16}$, (3) $2.5 \cdot 10^{16}$, (4) $5.0 \cdot 10^{16}$, and (5) $7.5 \cdot 10^{16}$ ion/cm^2. The spectrum taken from silica glass irradiated by silver ions $5.0 \cdot 10^{16}$ ion/cm^2 is shown for comparison.

on wide diffuse faint rings from the amorphous polymer matrix. By comparing the experimental diffraction patterns with standard ASTM data, it is possible to conclude that implantation does not form any chemical compounds involving silver ions.

From RBS spectra (Fig. 5), it is seen that the silver implantation layer (i.e., the depth where the nanoparticles are located) is almost independent of the ion dose. The dose dependence is observed only for the silver peak RBS intensities with the widths and positions of the lines remaining unchanged. It is known that the implantation depth of an ion depends largely on its energy (accelerating voltage) [5] if the chemical constitution of the surface irradiated does not change dramatically [52]). The similarity of the RBS spectra shown in Fig. 5 implies that the arising MN does not restrict the penetration depth of silver ions at the higher dose. Thus, in PMMA, the implantation dose, being responsible for the amount of the implant, influences directly the MN size but does not affect the implant distribution profile at present conditions. As was noted above, the particles nucleate at a dose of ~10^{16} ion/cm^2 (low-dose implantation). For silver in PMMA, this dose provides MN with a size of about 2 nm. However, at a dose of $5.0 \cdot 10^{16}$ ion/cm^2 (Fig. 3), the particles grow to ~10 nm.

Experimental optical absorption spectra for PMMA irradiated by xenon and silver ions at various doses are shown in Fig. 6. It is evident that the xenon irradiation of PMMA does not produce nanoparticles; this fact also follows from the micrographs (Fig. 3). In Fig. 6a, as the xenon ion dose increases, the absorption of the polymer in the visible (especially in the close-to-UV) range also increases monotonically. This indicates the presence of radiation-induced structure defects in the PMMA. The absence of absorption bands in these spectral curves is noteworthy. The implantation of silver not only generates radiation-induced defects but also causes the nucleation and growth of MN. Therefore, along with the absorption intensity variation as in Fig. 6a, an absorption band associated with silver nanoparticles is observed (Fig. 6b). For the lowest dose, the peak of this band is near 420 nm and shifts to longer waves (up to 600 nm) with dose, with the band broadening significantly. The peak of this band is not high, although it is related to the SPR effect in the silver nanoparticles. The low intensity of SPR absorption is untypical for silver nanoparticles in PMMA and cannot be explained by the polymer environment of the particles. When silver particles were synthesized in PMMA by the convection technique [55], the SPR intensity was very high (Fig. 7), unlike that registered in our experiment. Nor can the weak SPR absorption be

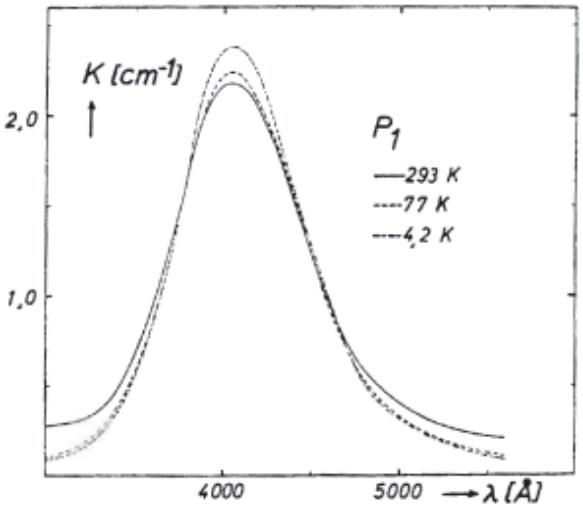

Fig. 7. Optical absorption of silver particles in PMMA fabricated by the convection technique and mastered at different temperature. Volume concentration of metal is $9\cdot10^{-7}$, data from [55].

explained by any features of the implantation process. For comparison, Fig. 4 shows the optical density spectrum for inorganic silica glass (SiO_2) irradiated by silver ions under the conditions used in this work for the ion synthesis (silica glass has the refractive index $n \approx 1.5$ close to that of PMMA) [52]. It is seen that the absorption of Ag nanoparticles in the glass (Fig. 6b) is much more intense (even in view of the background absorption due to matrix structure imperfections) than the absorption of the particles in the polymer. Note that the particle size distributions in the glass and PMMA are nearly the same. Below, the optical properties of the Ag–PMMA composite are simulated and various effects that may clarify the SPR absorption of Ag nanoparticles synthesized in PMMA by ion implantation are discussed.

4. MODELING OF OPTICAL EXTINCTION SPECTRA

4.1. Extinction of silver particles in dependence of environment matrix

The attenuation (extinction) of an optical wave propagating in a medium with MN depends on the amount of the SPR effect and the light scattering efficiency. The wavelength of optical radiation, the particle size, and the properties of the environment are governing factors in this process. Within the framework of classical electrodynamics (the Maxwell equations), the problem of interaction between a plane electromagnetic wave and a single spherical particle was exactly solved in terms of optical constants of the interacting objects by Mie [49,56]. According to the Mie theory, the extinction and scattering cross sections are expressed as an infinite sum of spherically symmetric partial electric and magnetic waves that generate fields similar to those generated by the particle when it is viewed as an excited multipole. The extinction cross section is generally given by

$$\sigma_{ext} = \frac{2\pi}{|\boldsymbol{k}|}\sum_{L=1}^{\infty}(2L+1)\,\mathrm{Re}(a_L + b_L), \qquad (3)$$

where $\boldsymbol{k}$ is the wavenumber and L is the order of spherical multipole excitation in the particle.

The case $L = 1$ corresponds to a dipole; $L = 2$ to a quadrupole; *etc*. The Mie coefficients a_L and b_L are expressed through the Riccati-Bessel cylindrical functions Ψ_L and η_L of variables mx or x, where $mx=\varepsilon_{Ag}/\varepsilon_{PMMA}$ is the ratio of the optical constants of the particles and polymer environment, and $x=|\boldsymbol{k}|R$ is the dimensional parameter, where R is the radius of the particle. These coefficients are given by [49,56]

$$a_L = \frac{m\Psi_L(mx)\Psi_L'(x) - \Psi_L'(mx)m\Psi_L(x)}{m\Psi_L(mx)\eta_L' - \Psi_L'(mx)\eta_L(x)}, \qquad (4)$$

$$b_L = \frac{\Psi_L(mx)\Psi_L'(x) - m\Psi_L'(mx)m\Psi_L(x)}{\Psi_L(mx)\eta_L' - m\Psi_L'(mx)\eta_L(x)}. \qquad (5)$$

In the general case, the Mie electromagnetic theory imposes no limitations on the wavelength of optical radiation. Therefore, the operation on the optical constants of the particles and matrix results in extinction spectra, so-called Mie resonance bands [2], which agree well with experiment. However, the Mie theory, which relies on the spectral dependence of the optical constants, does not allow one to penetrate deep into the physics of Mie optical peaks exhibited by the particles. Yet, independent investigations [2] of the behavior of silver nanoparticles showed that Mie resonances are due to the SPR effect, so that analytical Mie spectra may be compared with experimental data.

Extinction spectra for Ag nanoparticles embedded in a polymer matrix were computed and compared with experimental data shown in Fig. 6. In theoretical calculations, we used the complex value

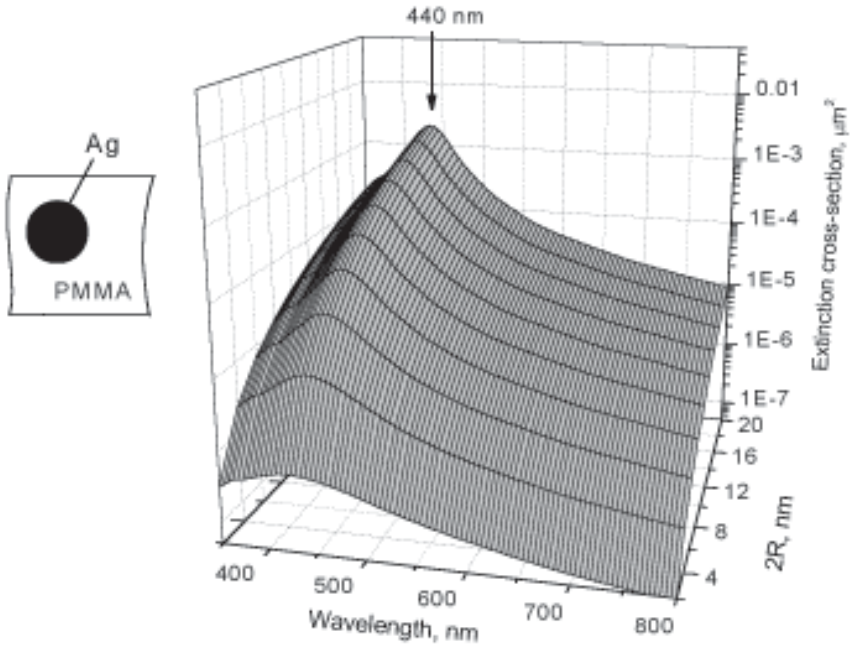

Fig. 8. Modelled optical extinction spectra for silver nanoparticles embedded in PMMA vs. particle size.

of the optical constant ε_{Ag} in the visible range [57] that was obtained by measurements on a set of fine silver particles. Such an approach [57] takes into account limitations imposed on the electron free path in particles of different size and electron scattering at the particle–insulator interface [58] and thus yields a more exact value of ε_{Ag} than the procedure of correcting optical constants for bulk silver [59]. The complex value of ε_{PMMA} for the polymer matrix were found elsewhere [50]. The extinction was calculated for particles of size between 1 and 10 nm (according to the MN sizes in Fig. 3).

At the early stage of simulation, consider the simple case where Ag nanoparticles are incorporated into the PMMA matrix. Associated extinction spectra for different metal particle sizes are shown in Fig. 8. These spectra feature a wide band, which covers the entire spectral range. In the given range of particle sizes, the position of the SPR absorption maximum (near 440 nm) is almost independent of the particle size. However, the extinction band intensity grows while the band itself somewhat narrows with increasing particle size. Comparing the analytical and experimental spectra, it is seen that, to the greatest extent, Fig. 8 refers to the situation where PMMA is irradiated by silver ions with doses between $0.33 \cdot 10^{16}$ and $2.5 \cdot 10^{16}$ ion/cm^2 (Fig. 6b, curves *1*–*3*). This dose range corresponds to the early stage of MN nucleation and growth in the *OD* spectral band with a maximum between 420 and 440 nm. Thus, one may conclude that ion implantation in this dose range results in the formation of Ag nanoparticles; this fact was also revealed microscopically. It may be supposed that radiation-induced defects in the PMMA have an insignificant effect on the MNP optical properties in this case. However, at higher implantation doses, the recorded OD spectra and the analytical spectra shown in Fig. 8 diverge; hence, the structure of the metal-polymer composite should be considered.

To explain the experimental dependences corresponding to high-dose silver implantation into PMMA, we will first elucidate the difference between implantation into polymers and inorganic insulators (silicate glasses, single crystals, minerals, *etc*.). The most important distinction is that, as the absorbed dose grows, so does the number of dangling chemical bonds along the track of an ion. Because of this, gaseous hydrogen, low-molecular hydrocarbons (e.g., acetylene), CO, and CO_2 evolve from the matrix [51]. In particular, ion-irradiated PMMA loses $HCOOCH_3$ methoxy groups [60]. The evolution of several organic fractions leads to the accumulation of carbon in the polymer layer irradiated, and radiation-induced chemical processes may cause chain linking. Eventually, an amorphous

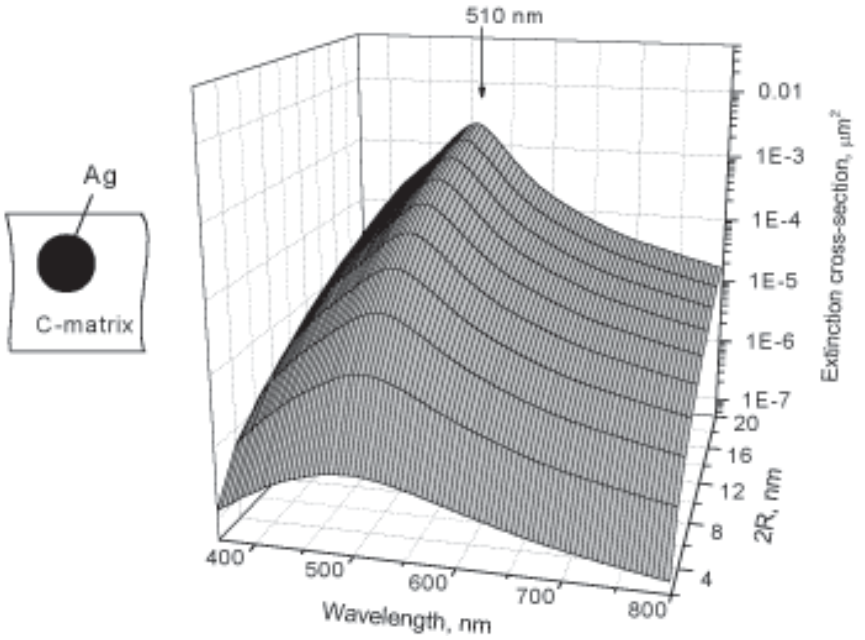

Fig. 9. Modelled optical extinction spectra for silver nanoparticles embedded in the C-matrix vs. particle size.

hydrogenated carbon layer is produced. Polymer carbonization starts with the formation of polycyclic compounds (in essence, primary carboniferous clusters) and, at higher doses, ends up with the formation of the well-developed carbonized phase via carbon cluster linking.

In view of the specific phase structure of the polymer irradiated, it is of interest to analyze the optical properties (extinction) of Ag nanoparticles embedded in the amorphous carbon matrix (C-matrix). For this system, the extinction cross section spectra vs. particle size dependence (Fig. 9) was simulated in the same way as for the MN–PMMA system, i.e., by using complex optical constants ε_C for amorphous carbon, which were taken from [61]. As before (Fig. 8), throughout the particle size interval, the extinction spectra exhibit a single broad band, which covers the visible range, with a peak at longer waves (510 nm). The calculated longwave shift of the peak, which is observed upon changing the matrix, may be assigned to a longer wave *OD* band in the experimental spectra for the PMMA, which arises when the Ag ion dose exceeds $2.5 \cdot 10^{16}$ ion/cm^2 (Fig. 6b; curves *3*, *4*). It seems that this spectral shift may be associated with the fact that the pure polymeric environment of the Ag nanoparticles turns into the amorphous carbon as the implantation dose rises. The broader extinction bands in the C-matrix (Fig. 9) compared with the PMMA (Fig. 8) also count in favor of this supposition, since the broadening of the extinction bands is observed in the experiments as well (Fig. 6b). In a number of experiments, however, the carbonization of the polymer surface layer depended on the type of the polymer and ion, as well as on the process parameters, and completed at doses of $(0.5–5.0) \cdot 10^{16}$ ion/cm^2 but the entire material was not carbonized. The carbon clusters may reach several tens of nanometers in size [62]. Thus, the assumption that the polymer irradiated is completely carbonized, which was used in the simulation (Fig. 9), does not meet the real situation when the process lasts for a long time. Below, the variation of the extinction spectra with amount of carbon in the PMMA layer is analyzed in terms of a model that considers the optical properties of silver MN covered by the amorphous carbon sheath.

4.2. Extinction of silver particles with carbon shell surrounded with polymer matrix

Extinction spectra for nanoparticles represented as a silver core covered by a carbon sheath in an insulating matrix (PMMA) will be analyzed in terms of the Mie relationships for sheathed cores [63]. Here,

an additional interface for which electrodynamic boundary conditions must be set up arises. Plasmon–polariton modes may be excited in both the core and the shell. These modes, interacting through the inner interface, are responsible for the resulting extinction spectrum. The Mie coefficients a_L and b_L for a homogenous sphere are replaced by associated expressions for a single spherical core with one shell [64,65]:

$$a_L = -\frac{m\Psi_L(mx)[\Psi_L'(x) + T_L\vartheta_L'(x)] - \Psi_L'(mx)\Psi_L(x)[\Psi_L(x) + T_L\vartheta_L(x)]}{m\xi_L(mx)[\Psi_L'(x) + T_L\vartheta_L'(x)] - \xi_L'(mx)[\Psi_L(x) + T_L\vartheta_L(x)]}, \tag{6}$$

$$b_L = -\frac{\Psi_L(mx)[\Psi_L'(x) + S_L\vartheta_L'(x)] - m\Psi_L'(mx)\Psi_L(x)[\Psi_L(x) + S_L\vartheta_L(x)]}{\xi_L(mx)[\Psi_L'(x) + S_L\vartheta_L'(x)] - m\xi_L'(mx)[\Psi_L(x) + S_L\vartheta_L(x)]}, \tag{7}$$

where the functions T_L and S_L are given by

$$T_L = -\frac{m\Psi_L(mx)[\Psi_L'(x) + \vartheta_L'(x)] - \Psi_L'(mx)\Psi_L(x)[\Psi_L(x) + \vartheta_L(x)]}{m\vartheta_L(mx)[\Psi_L'(x) + \vartheta_L'(x)] - \vartheta_L'(mx)[\Psi_L(x) + \vartheta_L(x)]}, \tag{8}$$

$$S_L = -\frac{\Psi_L(mx)[\Psi_L'(x) + \vartheta_L'(x)] - m\Psi_L'(mx)\Psi_L(x)[\Psi_L(x) + \vartheta_L(x)]}{\vartheta_L(mx)[\Psi_L'(x) + \vartheta_L'(x)] - m\vartheta_L'(mx)[\Psi_L(x) + \vartheta_L(x)]}. \tag{9}$$

Optical extinction spectra for an Ag nanoparticle with a fixed size of the core (4 nm) and a varying thickness of the carbon shell (from 0 to 5 nm) are shown in Fig. 10. The maximum of the SPR bands of the particles is seen to shift from 410 nm (uncovered particle, Fig. 8) to approximately 510 nm. Simultaneously, the SPR band intensity decreases, while the UV absorption increases, so that the absorption intensity at 300 nm and a shell thickness of 5 nm exceeds the SPR absorption of the particles. Both effects (namely, the shift of the SPR band to longer waves and the increased absorption in the near ultraviolet) agree qualitatively with the variation of the experimental optical density spectra (Fig. 6b) when the implantation dose exceeds $2.5 \cdot 10^{16}$ ion/cm^2. Thus, our assumption that the increase in the carbonized phase fraction with implantation dose and the variation of the optical density spectra (Fig. 6b) go in parallel is sustained by the simulation of the optical extinction for complex particles (sheathed cores, Fig. 10).

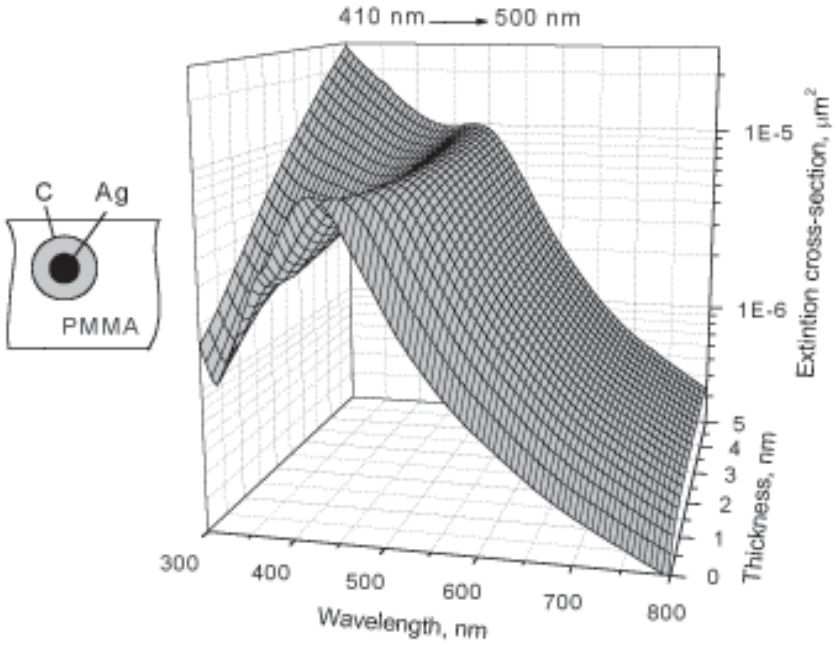

Fig. 10. Modelled optical extinction spectra for 4-nm silver nanoparticles with the carbon sheath that are placed in the PMMA matrix vs. sheath thickness.

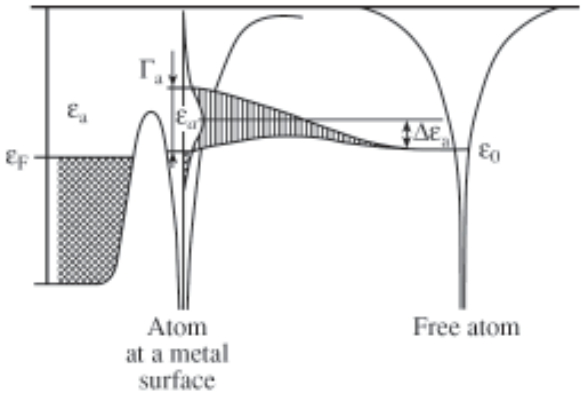

Fig. 11. Electron energy levels in an atom adsorbed on a metal surface. A free atom (to the right) reaches the surface (to the left). Γ_a is the spread of energy levels ε_a. Electron levels in the conduction band of the metal are occupied up to the Fermi level ε_f.

In spite of the fact that the model dependences on the carbon sheath thickness and the experimental dose dependences agree qualitatively, discrepancies still exist, particularly, in the position of the long-wave maximum in the optical density spectra and in the breadths of the simulated and experimental spectra. Possible reasons for such quantitative discrepancies are discussed below.

4.3. Interface effects in the silver core–carbon shell structure on optical extinction

Interest in carbon-based composites with MN goes back a long way. Examples are the studies of magnetic properties of cobalt particles [66], electric and optical properties of layers with copper [67] or silver [68,69] nanoparticles, *etc*. It was found in optical absorption experiments that copper and silver nanoparticles [67,69] dispersed in carbon matrices exhibit a weak SPR effect as in the present work (Figs. 6b, 6, 7).

When analyzing the optical properties of nanoparticles embedded in a medium, one should take into account effects arising at the particle–matrix interface, such as the static and dynamic redistributions of charges between electronic states in the particles and the environment in view of their chemical constitution [70].

Consider first the charge static redistribution. When an atom is deposited (adsorbed) on the MNP surface, the energy levels of this atom ε_a change their positions compared with those in the free state [70,71] (Fig. 11). When the number of the adsorbed matrix atoms becomes significant, their contact generates a wide distribution of density of states. Most frequently, the adsorbed atoms are separated from surface atoms of the metal by a tunnel barrier. The gap between the energy positions ε_a of the adsorbed atoms and the Fermi level ε_f of the particles depends on the type of the adsorbate (Fig. 11). In addition, the overlap between the energy positions of the matrix atoms and the energy positions of the silver surface atoms depends on the rate with which the electrons tunnel through the barrier. Accordingly, the conduction electron density in the particles embedded will change compared with that in the particles placed in a vacuum (without adsorbates): it decreases if the electrons tunnel toward the adsorbed atoms or increases when the electrons tunnel in the reverse direction. Eventually, equilibrium between the particle and the matrix sets in; i.e., a constant electrical charge (Coulomb barrier) forms at the nanoparticle surface.

Such a charge static redistribution due to the deposition of an adsorbate on the particle surface and the respective change in the electron concentration in the MN were also observed in the SPR absorption spectra [2,70]. In metals (silver, sodium, aluminum, *etc*.), where free conduction electrons dominate, the SPR spectral maximum $h\omega_{max}$ depends on the concentrations of electrons, *N*, and nanoparticles as

$$h\omega_{max} \approx \left[\frac{N}{\varepsilon_0 m_{eff}}\right]^{1/2} \left[2\varepsilon_m + 1 + \chi_1^{inter}\right]^{1/2}, \qquad (10)$$

where ε_m is the permittivity of the matrix, χ_1^{inter} specifies the contribution of the real part of the susceptibility of interband optical transitions in a metal, and m_{eff} is the effective mass of an electron.

It was shown [72] that the incorporation of Ag nanoparticles into the carbon matrix of C_{60} fullerene (or the deposition of carbon on the nanoparticle surface) reduces the concentration of 5sp electrons in the particle roughly by 20%, since they are trapped by matrix molecules. According to (10), the decrease in *N* is bound to shift the MN extinction spectrum toward longer waves, as also demonstrated by comparing the experimental spectra of the particles in free space (without an adsorbate) with those of the particles in the C_{60} matrix [72]. Samples studied in [72] were similar to those obtained by ion implantation in our work (a carbonized layer near silver particles implanted into the polymer). Thus, the shift of

the SPR extinction band into the longer wave range with implantation dose in this experiment (Fig. 6) may be explained by the formation of a carbon sheath around silver nanoparticles. This sheath traps conduction electrons of the particles. The simulation (Fig. 10) also demonstrates the shift of the SPR maximum. However, the effect of charge static redistribution is disregarded in the Mie theory. Therefore, the long-wave shift of the SPR band due to the charge static redistribution at the particle–matrix interface is an additional reason why the experimental spectra are observed at longer waves than the model ones (Figs. 9, 10).

Along with the charge static redistribution at the interface, the charge at the same interface may also change dynamically, i.e., with a high rate [70]. After the static state of the charge has been established and the Fermi level at the interface has been stabilized, the MN electrons optically excited above the Fermi level (hot electrons) may tunnel (by fluctuations) to the matrix over or through the static barrier (Fig. 11). Levels occupied by the electrons in the intermediate (between the particle and the matrix) state depend on the chemical constitution of the materials. Within a residence lifetime, the electrons may tunnel again from the acceptor levels of the matrix to the particle and this process may occur over and over.

The charge dynamic variation in time at the particle–matrix interface causes the electron concentration in the particle to fluctuate. Fluctuation influences directly the SPR relaxation. The lifetime of excited conduction electrons in the particle defines the SPR spectral width. Here, the contribution from electron scattering by the interface (because of restrictions imposed on the electron free path [2]) adds up with the charge dynamic variation at the interface. Thus, the temporal capture of conduction electrons from the particle broadens the SPR-related extinction spectra. This was demonstrated with a set of silver nanoparticles embedded in the C_{60} matrix [72]. Silver nanoparticles in the carbon matrix exhibit the much broader SPR band than in free space. We may therefore suppose that, as the dose rises, the charge dynamic redistribution may broaden the SPR spectra of silver nanoparticles synthesized by ion implantation in PMMA. This is because implantation carbonizes the irradiated layer with increasing absorbed dose and raises the amount of acceptor levels on the MNP surface, which change the relaxation time of electrons excited. Since the classical Mie theory disregards the charge dynamic redistribution, the model spectra (Fig. 10) must be narrower than the experimental spectra, which is the case.

5. OPTICAL ABSORPTION OF SILVER NANOPARTICLES PRODUCED IN VISCOUS POLYMER

In 1995 a new approach in ion implantation method for synthesis of metal nanoparticles based on irradiation of a viscous polymer was developed [28,29,32]. The use of the viscous relaxation state of the irradiated polymer offers the possibility of increasing the diffusion coefficient of the implanted ions by up to eight to ten orders of magnitude at room temperature [33]. After implantation, the viscous matrix transforms in to the solid-state as a result of polymerization processes and the synthesized MN are fixed in the volume of the substrate. Ion synthesis study on the formation of Co particles in viscous epoxy has shown that the size, morphology and crystalline structure of the metal particles can depend on the polymer viscosity [28-33].

In this section of paper some results of the optical properties of Ag nanoparticles synthesized by ion implantation in viscous organic matrix (silicone polymer resins) are demonstrated. In Fig. 12 (curves 1-4) we presented the optical transmittance spectra of the silicone polymer implanted at two doses of $3.0 \cdot 10^{16}$ and $1 \cdot 10^{17}$ ion/cm^2 into viscous (curves 1 and 2) and solid state substrate (curves 3 and 4). A

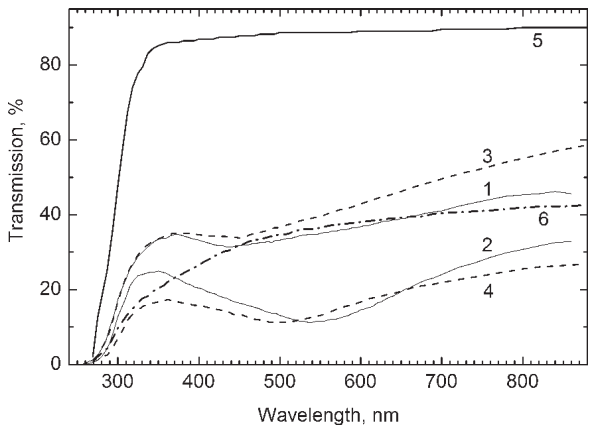

Fig 12. Optical transmission spectra of Ag-implanted viscous (curves 1 and 2) and solid state (curves 3 and 4) silicone polymer at doses of $0.3 \cdot 10^{17}$ ion/cm^2 (curves 1 and 3) and $1.0 \cdot 10^{17}$ ion/cm^2 (curves 2 and 4). Comparisons of the spectra of unirradiated silicone polymer (curve 5) and Ar-implanted solid polymer at a dose of $1.0 \cdot 10^{17}$ ion/cm^2 (curve 6) are presented [46].

selective minimum of the transmittance spectra at ~450 nm in matrices of both states, obtained at low doses, was detected. This absorption increases in amplitude and the band shifts toward longer wavelengths until 500 nm for solid state and until 550 nm for viscous state when the dose (the concentration of silver in polymer) is higher. The detected shift of bands for higher silver concentration is in consistency with result observed with Ag-implanted PMMA (Fig. 6).

The absorption in the implanted silicone polymer (Fig. 12) arises from two general sources: first, from structural defects introduced by the irradiation of organic matrix and, second, from the fabricated Ag MN. Similar to Xe-ion implantation into PMMA, the spectrum of the Ar-implanted silicone polymer (curve 6 in Fig. 12) demonstrates absorbance from radiation defects of organic matrix. Upon comparing spectra of the samples made by Ar- and Ag-ion implantation, it is possible to conclude that optical transmission (absorption) bands with peaks in the range from 350 to 700 nm are due to the formation of Ag particles. These bands are interpreted as SPR absorption in the small metal particles induced by electromagnetic radiation [2]. As in PMMA, dispersed isolated Ag ions and atoms do not exhibit such absorption in the visible range, and so the occurrence of selected peaks in the transmittance of the Ag-irradiated silicone polymer at a dose of 10^{16} ions/cm^2 (not present in Fig. 12) corresponds to the beginning of the formation of Ag MN during the ion implantation. Almost spherical particles were observed by TEM.

An unusually weak plasmon resonance absorption with very wide absorption bands observed in Ag-implanted solid state silicone polymer (curves 3 and 4 in Fig. 12), as in the case of PMMA, can be explained by strong carbonization of irradiated organic matrix which will reduce SPR in the Ag nanoparticles. However, as seen in same figure, the SPR absorption of MN synthesized in viscous polymer is characterized by sharper and strong resonance absorption bands than in solid state (curves 1 and 2). This spectral difference can be explained by formation of various carbon structures inside irradiated polymer. It can be suggested that in viscous organic matrix the carbonization process is less effective then during ion implantation of solid state polymers and so SPR of silver particles does not feel influence from carbon surrounding.

6. OPTICAL PROPERTIES OF METAL NANOPARTICLES IMPLANTED INTO DIFFERENT SOLID POLYMERS

In 2003 a study of metal nanoparticle fabrication in polymers by low energy negative ion implantations was started in National Institute for Materials Science (Japan) [35,36]. As was mentioned by the authors, application of negative ions to polymers, which are mostly insulating, has a merit to conduct implantation without surface charging and with the low processing temperature. They were focused on metal precipitation in comparison among various polymers. The creation of metal nanoparticles was controlled by the optical absorption and TEM analysis.

Organic specimens used were films of polyethylene (PE), polystyrene (PS) and polycarbonate (PC) of about 100 mm in thickness. Selected polymers have different chemical bonding structures and compositions, which was practically due to an amount of carbon atoms. The PE is a linear chain polymer, while the PS contains an aromatic ring. Their chemical formulas are $(CH_2)_n^-$ and $(CH_2CHC_6H_5)_n^-$, respectively. The PC contains aromatic rings and has oxygen in addition to hydrogen and carbons.

Fig. 13 demonstrates optical absorption spectra of PE, PS and PC irradiated with 60 keV Cu-ions to various total doses. At low doses, the absorbance monotonically increases with photon energy and this is primarily due to radiation-induced defects [35]. A distinct peak appears near 2 eV for PE and PS specimens above a dose $1.0 \cdot 10^{17}$ ion/cm^2. On the other hand, the peak appears at low doses for the PC specimen of $6.0 \cdot 10^{16}$ ion/cm^2. The existence of the peak near 2 eV indicates the implanted Cu atoms precipitate into metal particles, because this peak position agrees with well known optical absorption spectra for Cu nanoparticles in silicate glasses [2]. The formation of copper particles in the polymer volume is also evidenced by cross-section TEM image (Fig. 14). The larger Cu spheres of 5-10 nm in diameter are located at 40 nm distant from the surface and fine dots appear in the deeper region.

It should be mention that, as was shown above, a formation of silver nanoparticles in PMMA or silicone polymer takes place at lower ion doses. Nevertheless, in general, the dose dependences on optical properties of Cu-ion implanted polymer can be compared with Ag implanted samples.

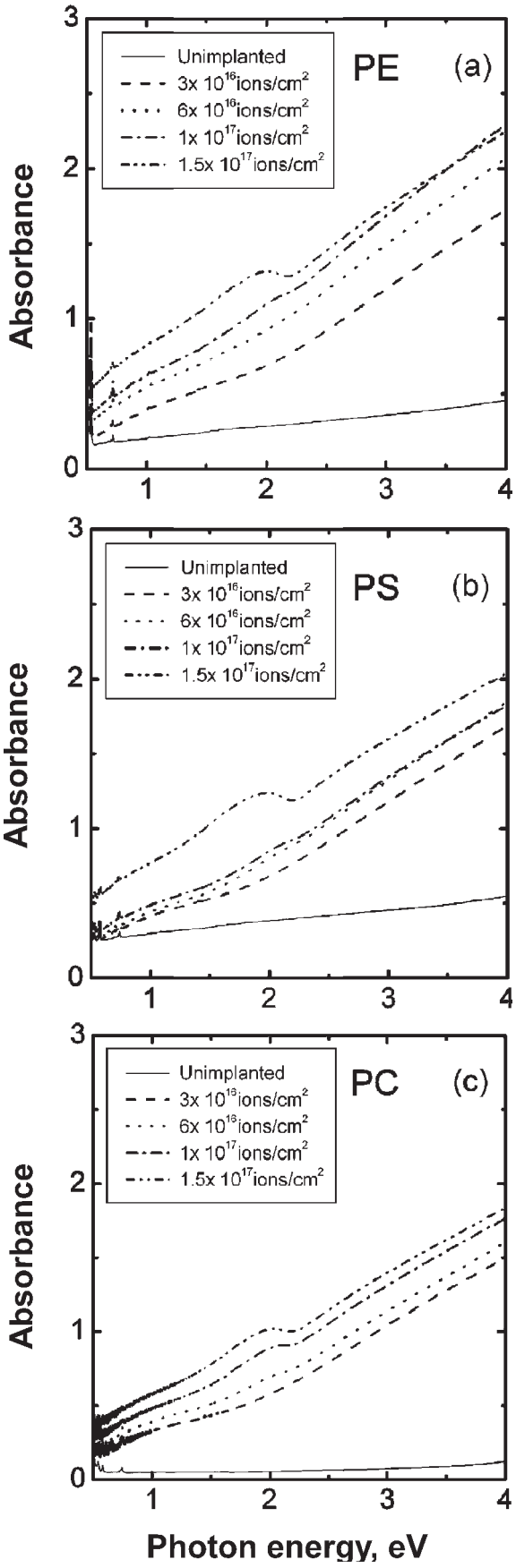

Fig. 13. Optical absorption spectra of unimplanted and implanted polymers of PE (a), PS (b) and PC (c) with 60 keV Cu-ions at 1 μA/cm^2, replotted from [35].

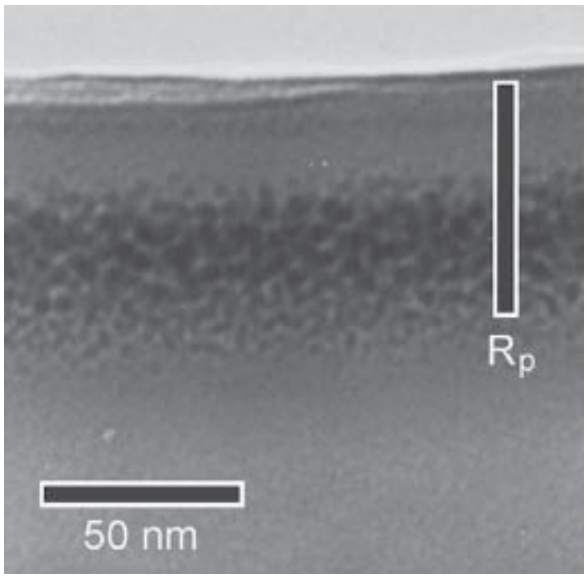

Fig. 14. Cross-sectional TEM image of PC specimen implanted with 60 keV Cu-ions at 1 μA/cm^2 to a dose of 1.5·10^{17} ion/cm^2. The R_p denotes a projected range of the Cu ions. Fragment of image with nanoparticles is taken with contrast correction form [35].

From the optical spectra (Fig. 13), authors concluded that the critical Cu concentration for precipitation is indeed smaller for the PC specimen than for the others. It was mentioned that the possible explanations for the stronger tendency may be associated with the higher radiation resistance of PC. Unfortunately, it is not completely clear that it means radiation resistance in contents of metal particle formation and their optical properties. However, we believed that one of the reasons for difference in absorbance is connected with the carbonization of implanted polymer and fabrication carbon environment around Cu nanoparticles, as it was discussed before.

ACKNOWLEDGEMENTS

A.L.S. is grateful to the Alexander Humboldt Foundation for the financial support of his work in Germany and Austrian Scientific Foundation in the frame of Lisa Meitner Fellowship. R.I.K. acknowledges support by NANO-TUBITAK PC-B Fellowship Programme (Turkey). This study was sponsored in part by the Federal Program for Support of the Leading Scientific Schools of Russia (project no. NSh 1904.2003.2) and by the OFN Russian grant 'Novel Materials and Structures'. Our special thanks to V.F.

Valeev, V.I. Nuzhdin, Yu.N. Osin and S.N. Abdullin (Kazan Physical-Technical Institute, Russia) for the assistance in carrying out implantation and electron microscopy study and also to D.E. Hole (University of Sussex, United Kingdom) for taking RBS spectra.

REFERENCES

[1] C. Flytzanis, F. Hache, M. C. Klein, D. Ricard and P. Rousignol, *Nonlinear optics in composite materials* (Elsevier Science, Amsterdam, 1991).

[2] U. Kreibig and M. Vollmer, *Optical properties of metal clusters* (Springer-Verlag, Berlin, 1995).

[3] S.N. Abdullin, A.L. Stepanov, Yu.N. Osin and I.B. Khaibullin // *Surf. Sci*. **395** (1998) L242.

[4] M. Quinten, A. Heilmann and A. Kiesow // *Appl. Phys. B* **68** (1999) 707.

[5] P.T. Townsend, P.J. Chandler and L. Zhang, *Optical effects of ion implantation* (Cambridge Univ. Press, Cambridge, 1994).

[6] J. Davenas, A. Perez, P. Thevenard, and C.H.S. Dupuy // *Phys. Stat. Sol. A* **19** (1973) 679.

[7] G.W. Arnold // *J. Appl. Phys.* **46** (1975) 4466.

[8] N.C. Koon, D. Weber, P. Pehrsson and A.I. Sindler // *Mater. Res. Soc. Symp. Proc.* **27** (1984) 445.

[9] Y. Wu, T. Zhang, Y. Zhang, H. Zhang, H. Zhang and G. Zhou // *Nucl. Instr. Meth. B* **173** (2001) 292.

[10] T.-H. Zhang, Y.-G. Wu, H.-B. Sang, Y.-L. Li, G. Zhou // *Chinese Phys*. **10** (2001) 295.

[11] Y. Wu, T. Zhang, H. Zhang, X. Zhang, Z. Deng and G. Zhou // *Nucl. Instr. Meth. B* **169** (2000) 89.

[12] K. Ogawa, *U.S. Pat*. 4,751,100 (1988).

[13] V.Yu. Petukhov, M.I. Ibragimova, N.P. Khabibullina, S.V. Shulyndin, Yu.N. Osin, E.P. Zheglov, T.A. Vakhonina and I.B. Khaibullin // *Polymer Sci. A* **43** (2001) 1154. Translated from *Vysokomolekulyarnye Soedinenia A* **43** (2001) 1973, in Russian.

[14] R.I. Khaibullin, V.N. Popok, V.V. Bazarov, E.P. Zheglov, B.Z. Rameev, C. Okay, L.R. Tagirov and B. Aktas // *Nucl. Instr. Meth. B* **191** (2002) 810.

[15] V.N. Popok, R.I. Khaibullin, V.V. Bazarov, V.F. Valeev, V. Hnatowicz, A. Mackova and V.B. Odzhaev // *Nucl. Instr. Meth. B* **191** (2002) 695.

[16] V.N. Popok, R.I. Khaibullin, A. Toth, V. Beshliu, V. Hnatowicz and A. Mockova // Surf. Sci. **532-535** (2003) 1034.

[17] B.Z. Rameev, F. Yildiz, B. Aktas, C. Okay, R.I. Khaibullin, E.P. Zheglov, J.C. Pivin, L.R. Tagirov // Micr. Engin. **69** (2003) 330.

[18] V.Yu. Petukhov, V.A. Zhikharev, N.R. Khabibullina and I.B. Khaibullin // *Vysokochist. Veshchestva* **3** (1993) 45, in Russian.

[19] V.Yu. Petukhov, V.A. Zhikharev, I.F. Makovskii, Yu.N. Osin, M.A. Mitryaikina, I.B. Khaibullin and S.N. Abdullin // *Poverhnost* **4** (1995) 27, in Russian.

[20] V. Petukhov, V. Zhikharev, M. Ibragimova, E. Zheglov, V. Bazarov and I. Khaibullin // *Solid State Comm*. **97** (1996) 361.

[21] V.V. Bazarov, V.Yu. Petukhov, V.A. Zhikharev and I.B. Khaibullin // *Mater. Res. Soc. Symp. Proc*. **388** (1995) 417.

[22] R.I. Khaibullin, Yu.N. Osin, A.L. Stepanov and I.B. Khaibullin // *Vacuum* **51** (1998) 289.

[23] R.I. Khaibullin, Yu.N. Osin, A.L. Stepanov and I.B. Khaibullin // *Nucl. Instr. Meth. B* **148** (1999) 1023.

[24] R.I. Khaibullin, V.A. Zhikharev, Yu.N. Osin, E.P. Zheglov, I.B. Khaibullin, B.Z. Rameev and B. Aktas // *Nucl. Instr. Meth. B* **166-167** (2000) 897.

[25] R.I. Khaibullin, B.Z. Rameev, V.N. Popok, E.P. Zheglov, A.V. Kondyurin, V.A. Zhikharev, B. Aktas // Nucl. Instr. Meth. B **206** (2003) 1115.

[26] B.Z. Rameev, B. Aktas, R.I. Khaibullin, V.A. Zhikharev, Yu.N. Osin and I.B. Khaibullin // *Vacuum* **58** (2000) 551.

[27] A.L. Stepanov, R.I. Khaibullin, S.N. Abdullin, Yu.N. Osin and I.B. Khaibullin // *Mater. Res. Soc. Symp. Proc.* **343** (1994) 161.

[28] A.L. Stepanov, R.I. Khaibullin, S.N. Abdullin, Yu.N. Osin, V.F. Valeev and I.B. Khaibullin // *Pros. Inst. Phys. Conf. Ser*. **147** (1995) 357.

[29] S.N. Abdullin, A.L. Stepanov, R.I. Khaibullin, F.V. Valeev, Yu.N. Osin and I.B. Khaibullin // *Phys. Solid State* **38** (1996) 1412. Translated from *Fizika Tverdogo Tela* **38** (1996) 2574, in Russian.

[30] S.N. Abdullin, A.L. Stepanov, R.I. Khaibullin and I.B. Khaibullin, *Rus. Feder. Pat*. 2096835 (1996).

[31] S.N. Abdullin, A.L. Stepanov, Yu.N. Osin, R.I. Khaibullin and I.B. Khaibullin // *Surf. Coat. Techn.* **106** (1998) 214.

[32] R.I. Khaibullin, C.N. Abdullin, A.L. Stepanov, Yu.N. Osin and I.B. Khaibullin // *Tech. Phys. Lett*. **22** (1996) 112. Translated from *Pis'ma v Zhurnal Technicheskoi Fiziki* **22** (1996) 48, in Russian.
[33] I.B. Khaibullin, R.I. Khaibullin, S.N. Abdullin, A.L. Stepanov, Yu.N. Osin, V.V. Bazarov and S.P. Kurzin // *Nucl. Instr. Meth. B* **127-128** (1997) 685.
[34] B. Rameev, C. Okay, F. Yildiz, R.I. Khaibullin, V.N. Popok and B. Aktas // *J. Magn. Mag. Mat.* 278 (2004) 164.
[35] N. Umeda, V.V. Bandourko, V.N. Vasilets and N. Kishimoto // *Nucl. Instr. Meth. B* **206** (2003) 657.
[36] H. Boldyryeva, N. Kishimoto, N. Umeda, K. Kono, O.A. Plaksin and Y. Takeda // *Nucl. Instr. Meth. B* **219-220** (2004) 953.
[37] Y. Wu, T. Zhang, Y. Zhang, G. Zhou, H. Zhang and X. Zhang // *Surf. Coat. Techol*. **148** (2001) 221.
[38] K. Yoshida and M. Iwaki // *Nucl. Instr. Meth. B* **19-20** (1987) 878.
[39] T. Kobayashi, T. Iwata, Y. Doi and M. Iwaki // *Nucl. Instr. Meth. B* **175-177** (2001) 548.
[40] A.L. Stepanov, S.N. Abdullin, R.I. Khaibullin, V.F. Valeev, Yu. N. Osin, V.V. Bazarov and I.B. Khaibullin // *Mater. Res. Soc. Symp. Proc.* **392** (1995) 267.
[41] A.L. Stepanov, S.N. Abdullin, R.I. Khaibullin and I.B. Khaibullin, *Rus. Feder. Pat.* 97 109708 (010137) (1997).
[42] Y. Wu, T. Zhang, A. Liu and G. Zhou // *Surf. Coat. Techol*. **157** (2002) 262.
[43] A.L. Stepanov, S.N. Abdullin, R.I. Khaibullin, Yu.N. Osin and I.B. Khaibullin // *Proc. Roy. Micr. Soc.* **29** (1994) 226.
[44] A.L. Stepanov, S.N. Abdullin, V.Yu. Petukhov, Yu.N. Osin, R.I. Khaibullin and I.B. Khaibullin // *Phil. Mag. B* **80** (2000) 23.
[45] A.L. Stepanov, V.N. Popok, I.B. Khaibullin and U. Kreibig // *Nucl. Instr. Meth. B* **191** (2002) 473.
[46] A.L. Stepanov, R.I. Khaibullin and I.B. Khaibullin // *Phil. Mag. Lett*. **77** (1998) 261.
[47] Y. Wu, T. Zhang, A. Liu, X. Zhang and G. Zhou // Vacuum **69** (2003) 461.
[48] G.R. Rao, K. Monar, E.H. Lee and J.R. Treglio // *Surf. Coat. Technol*. **64** (1994) 69.
[49] G. Mie // *Ann. Phys. (Leipzig)* **25** (1908) 377.
[50] M.A. Khashan and A.Y. Nassif // *Opt. Comm.* **188** (2001) 129.
[51] D.V. Sviridov // *Russian Chem. Rev.* **71** (2002) 315.
[52] A.L. Stepanov and D. E. Hole // *Recent Res. Devel. Applied Phys.* **5** (2002) 1.
[53] V.B. Odzhaev, I.P. Kozlov, V.N. Popok and D.V. Sviridov, *Ion implantation into polymers* (Belarusk. Gos. Univ., Minsk, 1998) , in Russian..
[54] S. Deying, Y. Saito and S. Suganomata // *Jpn. J. Appl. Phys.* **33** (1994) L966.
[55] W. Scheunemann and H. Jäger // *Z. Phys.* **265** (1973) 441.
[56] C.F. Bohren and D.R. Huffman, *Absorption and scattering of light by small particles* (Wiley, New York 1983).
[57] M. Quinten // *Z. Phys. B* **101** (1996) 211.
[58] U. Kreibig // *J. Phys. F* **4** (1974) 999.
[59] P.B. Johnson and R.W. Christy // *Phys. Rev. B* **6** (1972) 4370.
[60] B. Pignataro, M. E. Fragala and O. Puglisi // *Nucl. Instr. Meth. B* **131** (1997) 141.
[61] E. D. Palik, *Handbook of optical constants of solids* (Academic, London, 1997).
[62] G.R. Rao, Z.L. Wang and E.H. Lee // *J. Mater. Res*. **8** (1993) 927.
[63] A. Aden and M. Kerker // *J. Appl. Phys.* **22** (1951) 1242.
[64] J. Sinzig, U. Radtke, M. Quinten and U. Kreibig // *Z. Phys. D* **26** (1993) 242.
[65] J. Sinzig and M. Quinten // *Appl. Phys. A* **58** (1994) 157.
[66] H. Wang, S.P. Wong, W.Y. Cheung, N. Ke, M.F. Chiah, H. Liu and X.X. Zhang // *J. Appl. Phys.* **88** (2000) 2063.
[67] V.I. Ivanov-Omskii, A.V. Tolmatchev and S.G. Yastrebov // *Philos. Mag. B* **73** (1996) 715.
[68] H. Biederman, Z. Chmel, A. Fejfar, M. Misina and J. Pesicka // *Vacuum* **40** (1990) 377.
[69] O. Stenzel, H. Kupfer, T. Pfeifer, A. Lebedev and S. Schulze // *Opt. Mater.* **15** (2000) 159.
[70] U. Kreibig, *Handbook of optical properties*, Vol. 2: *Optics of small particles, interfaces, and surfaces*, Ed. By R.E. Hummel and P. Wissmann, (CRC, London, 1997).
[71] J. Hölzl, F. Schulte and H. Wagner, *Solid surface physics* (Springer, Berlin, 1979).
[72] U. Kreibig, M. Gartz and A. Hilger // *Ber. Bunssenges. Phys. Chem.* **101** (1997) 1593.